Journal of
Mechanics of
Materials and Structures

# INFLUENCE OF MATRIX PLASTICITY AND RESIDUAL THERMAL STRESS ON INTERFACIAL DEBONDING OF A SINGLE FIBER COMPOSITE

Yi Pan and Assimina A. Pelegri

Volume 5, Nº 1 January 2010

mathematical sciences publishers

JOURNAL OF MECHANICS OF MATERIALS AND STRUCTURES
Vol. 5, No. 1, 2010

# INFLUENCE OF MATRIX PLASTICITY AND RESIDUAL THERMAL STRESS ON INTERFACIAL DEBONDING OF A SINGLE FIBER COMPOSITE

YI PAN AND ASSIMINA A. PELEGRI

Fiber/matrix interfacial debonding in a single short-fiber reinforced polymer composite is investigated using finite elements and a cohesive zone model. The glass fiber is modeled as an isotropic, linear elastic material. The matrix is modeled as a linear elastic/elastoplastic material characterized by incremental isotropic hardening. A cohesive zone model governed by the traction-separation law describes the fiber/matrix interface. The simulated stress field of the single fiber debonded and perfectly bonded composites are compared. The results indicate that the interfacial shear stress decreases to zero on the debonded interface. It increases to its maximum value over a small processing zone and decreases exponentially to zero at the fiber midpoint. The debonding length growth in the plastic model is larger than that in the elastic model at small applied strain levels, but the trend is reversed as the applied strain level increases. The influence of factors such as residual thermal stress, interfacial strength, and fracture toughness on the debonding process of a single fiber composite are discussed.

## 1. Introduction

Fiber/matrix interfacial properties and the mechanical properties of the matrix are key factors that influence the stress-strain behavior and fracture toughness of short fiber reinforced composites (SFRC) [Mandell et al. 1982; Norman and Robertson 2003]. Fiber/matrix interfacial debonding is one of the primary damage mechanisms in the fragmentation test of a single fiber composite (SFC) [Cheng et al. 1993; Galiotis 1993; Yallee and Young 1998; Kim and Nairn 2002] and in the fracture test of random SFRCs [Mandell et al. 1982; Norman and Robertson 2003].

Galiotis [1993] has demonstrated that the load transfer mechanism in fiber reinforced composites is activated in the vicinity of discontinuities such as fiber ends and fiber breaks. In the case of SFRCs with fiber axes parallel to the direction of loading, the mechanism of load transfer from the matrix to the fiber is through interfacial shear stress. Fiber/matrix interfacial debonding, governed by the interfacial shear strength (IFSS) and fracture toughness, changes the stress transfer mechanism in the composite by altering the stress field around the fiber. Furthermore, Kim and Nairn [2002] observed that interfacial debonding occurred simultaneously with fiber breakage when they performed fragmentation tests on continuous SFCs. They also noted that further increases in the applied strain resulted in debonding propagation.

The determination of interfacial properties through an analysis of the stress field around a discontinuous fiber has been thoroughly studied [Galiotis 1993; Yallee and Young 1998; Kim and Nairn 2002]. It was reported that the number of instantaneous debonded interfaces accompanied by fiber breakage

*Keywords:* interfacial debonding, finite element analysis, single fiber composite, interfacial strength, fracture toughness, matrix plasticity, residual thermal stress.

increased at low applied strains and then decreased at higher strains, while the total debonded length enlarged as the applied strain increased.

Analytical and numerical studies have been performed to determine the stresses in the fiber and along the fiber/matrix interface in a perfectly bonded discontinuous fiber composite. The shear-lag model [Cox 1952], widely applied in the fragmentation test in order to determine the interfacial strength and fracture toughness [Galiotis 1993; Yallee and Young 1998], predicts that the maximum interfacial shear stress occurs at both ends of a discontinuous fiber and it decreases exponentially to zero at the fiber midpoint. It also predicts that the minimum normal stress in the fiber occurs at both ends of the discontinuous fiber and increases exponentially to its maximum value at the midpoint.

Carrara and McGarry [1968] studied the stress field of a discontinuous fiber composite in order to identify the optimal fiber-end geometry that would minimize the matrix shear stress concentration. They ascertained that at the fiber-end the stress theoretically predicted by the Cox shear-lag model (which does not account for stress concentrations) is only about half of the value obtained using a FEM that incorporates the stress concentration effect.

Daoust et al. [1993] performed a finite element (FE) analysis on a SFC fragmentation test and modeled the fiber sizing (thin coating layer) as an interphase with low modulus. The soft interphase layer decreased the stress at the ends of the fragment. The effect became more prominent when the thickness of the interphase layer was increased. Daoust's group introduced the gap elements, which only transmit compressive stress, to describe fiber discontinuities due to fiber breakage. The stress field obtained in their model is more realistic than that predicted by the Cox analytical model.

All the aforementioned studies assume a perfectly bonded interface and elastic behavior for the fiber and matrix materials. For matrices with remarkable elastoplastic behavior, Tripathi et al. [1996] introduced matrix plasticity to their FEM to illustrate the limitations of that assumption. Without considering fiber/matrix interfacial debonding, these authors found that the shear stress value near the fiber-end forms a plateau with value less than the maximum shear stress at the interface. The length of this plateau is enlarged as the applied strain increases. Their work is useful in determining the IFSS when no fiber/matrix interface debonding occurs in a single SFC fragmentation test. However, the stress pattern changes and the stress field becomes more complex as partially and/or fully interfacial debonding occurs [Yallee and Young 1998; Kim and Nairn 2002].

In the present study, we model the interfacial debonding of a SFC by a cohesive element using ABAQUS 6.8. Matrix plasticity is accounted for by the elastoplastic model. The model follows the isotropic hardening rule within the framework of incremental theory, where it is assumed that the mechanical strain rate is decomposed into an elastic part and a plastic part. Residual thermal stress (RTS) prevails in the fiber reinforced polymer composite due to the mismatch of thermal expansion coefficients (CTEs) of the fiber and matrix. The effects of interfacial strength, interfacial fracture toughness, and RTS on the interfacial debonding are investigated.

## 2. Finite element model

The model consists of a cylindrical short fiber centered within a cylindrical matrix. The fiber and the matrix are assumed to be isotropic materials. The cylindrical composite is loaded with a uniform tensile displacement. Since the loading and the geometry are both axisymmetric and the interfacial debonding

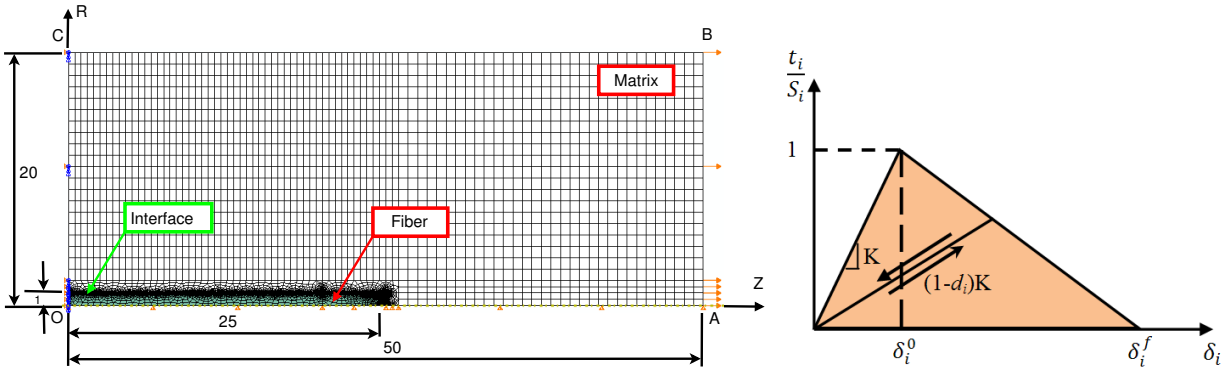


**Figure 1.** Schematic illustration of a single fiber embedded in the matrix (left, showing the finite element model) and of the traction-separation response (right).

on the lateral surface only undergoes mode II fracture, it is possible to model the physical problem using a two-dimensional axisymmetric model.

***Geometric model.*** The geometry and meshing are illustrated in Figure 1, left. $R$ is the radial direction and $Z$ is the direction of the axis of symmetry along the fiber's centerline. The problem is symmetric about the midplane perpendicular to the $Z$-axis. Symmetric boundary conditions are applied on the edge $OC$. Axisymmetric boundary conditions are applied to the fiber centerline, the edge $OA$. The edge $BC$ is a free edge. A uniform tensile displacement condition is applied on the edge $AB$. The radius of the fiber $r$ is of unit value and the total length of the fiber $l$ is equal to 50 (only one half of the fiber is shown due to symmetry). The radius of the cylindrical composite, $R_0$, is set to 20 and the composite length is twice the length of the fiber. A fictitious thin layer with thickness of 0.2% of the fiber radius is inserted between the fiber and the matrix to model the interface.

***Material properties and the mesh.*** A cohesive zone model using cohesive elements governed by the traction-separation law [Camanho and Dávila 2002; Camanho et al. 2003; Turon et al. 2005; 2007; ABAQUS 2008; Dávila et al. 2008] is employed to describe the interface. The four-node axisymmetric element, CAX4, is used for the fiber and the matrix, while the four-node axisymmetric cohesive element, COHAX4, is used for the interface. A fine mesh is applied on the vicinity of the fiber/matrix interface and the mesh becomes coarser away from the interface, see Figure 1, left. The fiber, the interface, and the matrix are meshed using 9746, 2080, and 10303 elements, respectively. A relatively coarse mesh (double the size of the mesh reported here) was also used to study the solution dependency on mesh size. Both the coarse mesh (not reported) and the fine mesh (reported) in this study converged to the same solution. The Young's modulus, $E_f$, and the Poisson's ratio, $\nu$, of the linearly elastic fiber are 72 GPa and 0.22, respectively. Two types of constitutive behavior of the epoxy matrix are used, one of which is the linear elastic behavior with $E_m = 3.22$ GPa and $\nu = 0.35$. The other is the elastoplastic behavior governed by the same the elastic constants as the linear elastic behavior, a von Misses yield surface, and the isotropic hardening rule [ABAQUS 2008]. Even though the polymers in general have higher compressive yield strengths than tensile yield strengths and their hydrostatic stress dependent yielding behavior may be represented more precisely with other models such as the Drucker–Prager model, one

may use von Misses yield criterion to predict the yield point of epoxy resins with acceptable accuracy. That is because the hydrostatic stress is not prominent in the loading cases in this study. The strain hardening curve for elastoplastic epoxy resin input into ABAQUS is shown in Figure 2; the data is from [Tripathi et al. 1996]. The predicted stress/plastic strain curve is in good agreement with the experimental data.

***Bilinear traction-separation law.*** The traction-separation law, one of the constitutive behaviors available for the cohesive element, was described in great detail in [ABAQUS 2008, Section 27.5]. It relates the traction to the displacement jump (separation) across the interface. The bilinear softening model is shown in Figure 1, right, and can be defined as

$$t_i = \begin{cases} K\delta_i, & \text{if } \delta_i^{\max} \le \delta_i^0, \\ (1-d_i)K\delta_i, & \text{if } \delta_i^0 < \delta_i^{\max} < \delta_i^f, \\ 0, & \text{if } \delta_i^{\max} = \delta_i^f, \end{cases} \tag{2-1}$$

and

$$d_i = \frac{\delta_i^f(\delta_i^{\max} - \delta_i^0)}{\delta_i^{\max}(\delta_i^f - \delta_i^0)}, \qquad i = 1, 2, 3, \quad d_i \in [0, 1], \tag{2-2}$$

where $t$ and $\delta$ are the traction and separation of the interface, respectively. The subscript $i$ refers to the normal loading and the first and second shear loadings, respectively. The initial response is linear, characterized by the penalty stiffness $K$ with no damage. After the interfacial normal, or the shear, tractions attain their corresponding interfacial tensile, or shear strengths, the stiffness is gradually reduced to zero. The damage onset separations can be computed as: $\delta_i^0 = S_i/K$, where $S_1$, $S_2$, and $S_3$ are the interfacial tensile strength and the interfacial shear strength in the first and the second shear directions, respectively. The area under the traction-separation curves is the corresponding mode I, II, and III fracture

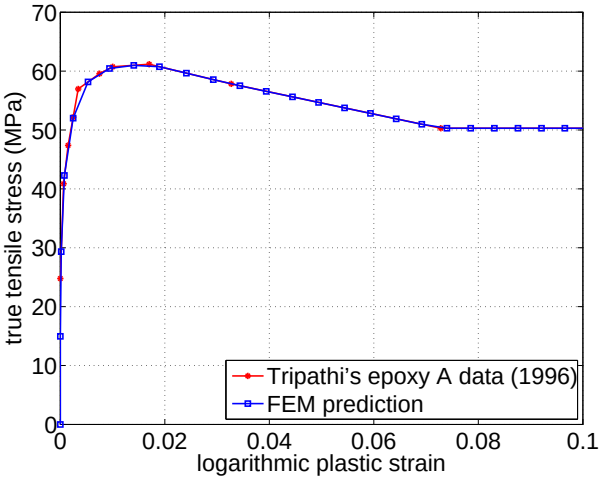


**Figure 2.** Strain hardening curve for epoxy resin.

toughness, $G_{\mathrm{IC}}$, $G_{\mathrm{IIC}}$ and $G_{\mathrm{IIIC}}$, respectively. The final separations can be defined as

$$\delta_1^f = 2G_{\mathrm{IC}}/S_1, \quad \delta_2^f = 2G_{\mathrm{IIC}}/S_2, \quad \delta_3^f = 2G_{\mathrm{IIIC}}/S_3.$$

The variable $d_i$, denoting the corresponding damage state, depends on the maximum separation, $\delta_i^{\max}$, attained during the loading history.

## 3. Finite element results and comparison to shear-lag model prediction

Galiotis [1993], Yallee and Young [1998], and Kim and Nairn [2002] found in experiments that partial or full interfacial debonding occurs in fragmentation test of SFCs due to the high interfacial shear stress at the tip of embedded short fibers or broken fibers. The IFSS, on the order of $\sim$10 to $\sim$100 MPa for the glass (or carbon) fiber/epoxy system in which we are interested, depends greatly on the fiber/matrix system and the fiber's surface treatment. The critical interfacial fracture energy is approximately 100 J/m$^2$. A penalty stiffness of $K = 10^6$ N/mm$^3$ is used for the traction-separation law. Guidelines for determining $K$ can be found in [Turon et al. 2007]. The effect of matrix properties on the stress field of a SFC is being studied here by using the linear elastic and the isotropic hardening plastic models. The uncoupled traction-separation law is applied in our study. Damage initiation is governed by the maximum stress criterion, and damage evolution is governed by the effective displacement, $\delta_i^f$, at complete failure of the interfacial layer modeled by the cohesive element [ABAQUS 2008]. Results of the FE simulations and the shear-lag predictions of the perfectly bonded interface model are also compared to those of the debonding interface model. The effects of residual thermal stress are addressed in Section 4.

***Finite element results.*** Finite element results of the elastic and the elastoplastic matrix models with a perfectly bonded interface and a debonding interface are presented in this section. Two phenomena are investigated: damage initiation, when damage of the first interfacial cohesive element starts, which is governed by the strength, and crack initiation, when total failure of the first interfacial cohesive element occurs, which is governed by the interfacial fracture toughness.

*Perfectly bonded interface model.* In the case of a perfectly bonded interface, the fiber axial stress and the interfacial shear stress obtained from the FE analysis are shown in Figure 3. In the case of the elastic matrix model, both the interfacial shear stress (top left) and the axial stress (top right) in the fiber increase with the applied strain at the fiber tip. The fiber axial stress attains its maximum at the fiber midpoint and the interfacial shear stress decreases along the length of the fiber and reduces to zero at the fiber midpoint. For the model with the elastoplastic matrix, the shear stress profile (Figure 3, bottom left) almost coincides with the elastic model at small applied strains (less than 0.6%) except the small region around the fiber end. At higher applied strains, it is observed that the shear stress value near the fiber end forms a plateau and the value of the plateau is less than the maximum shear stress at the interface. The length of this plateau is enlarged as the applied strain increases. Similar results were reported in [Termonia 1987] for the elastic matrix model and in [Tripathi et al. 1996] for the elastoplastic matrix model. The results are presented here for the purpose of completeness and comparison to the debonding interface model. Due to the plateau of the interfacial shear stress, the fiber axial stress (Figure 3, bottom right) is almost linear in that region since the axial load in the fiber is transferred by the interfacial shear stress.

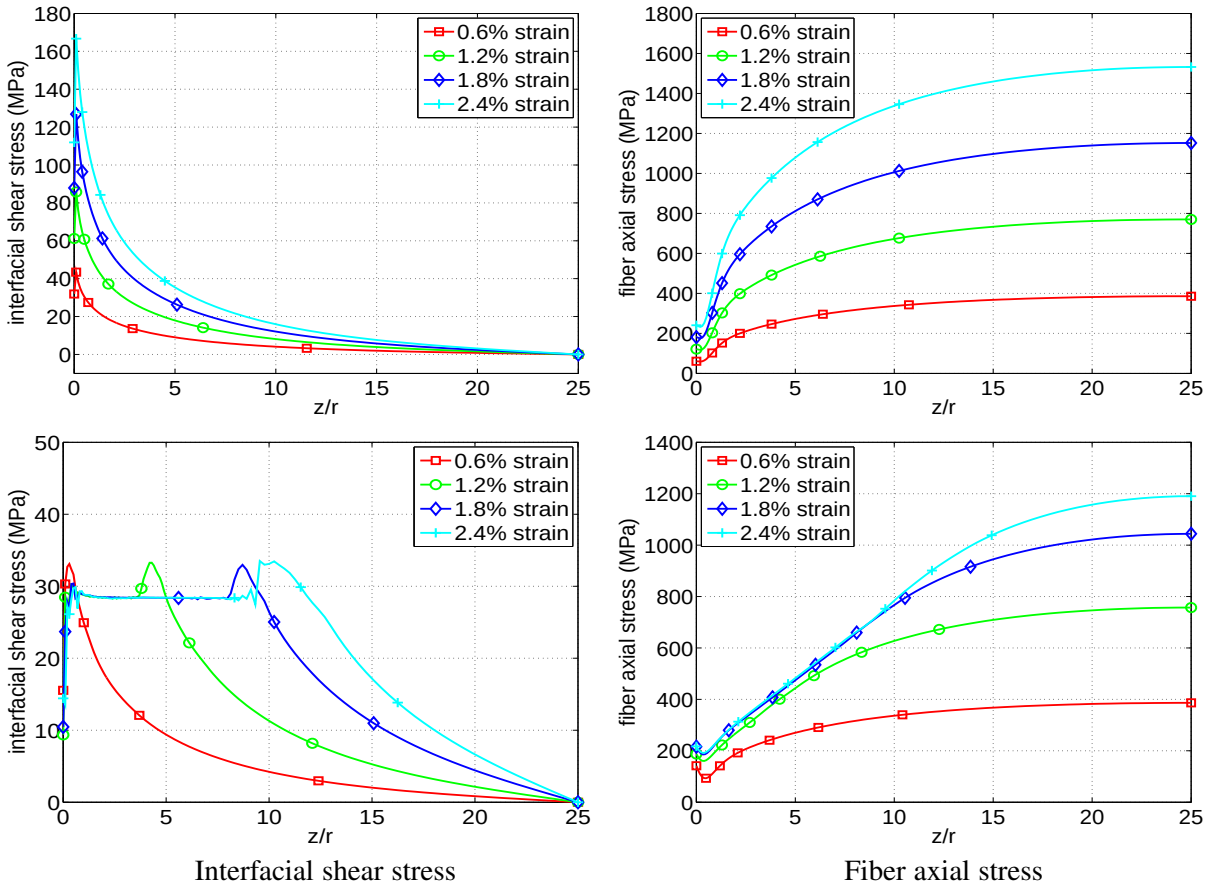


**Figure 3.** Interfacial shear stress (left column) and fiber axial stress (right column) of FEM results of perfectly bonded interface model with elastic matrix (top) and elastoplastic matrix (bottom).

*Interfacial debonding model.* Stress concentration at fiber ends due to the fiber-end geometry [Carrara and McGarry 1968] and material mismatch results in interfacial debonding. Stress/strain profiles change greatly when interfacial debonding is accounted for, compared to the perfectly bonded interface model. The interfacial shear stress profiles and fiber axial stress profiles are shown in Figure 4.

A disparity between the stress profiles of the debonding and the perfectly bonded models is observed. In the interfacial debonding model ($S_2 = 20\,\text{MPa}$, $G_{\text{IIC}} = 100\,\text{J/m}^2$) the shear stresses on the debonded interface reduce to zero when the interfacial debonding occurs (a fully damaged interface, meaning the damage variable $d$ is equal to 1 at all integration points). It increases from zero to its maximum value over the damage processing zone, where the damage of the cohesive element is activated ($0 < d < 1$), see Figure 4, left. At the fiber tip, the axial stresses increase with the applied strain only before the interfacial debonding initiates. At a certain applied strain, at which the interfacial shear stress equals the interfacial strength, interfacial damage occurs. The axial stresses at the fiber tip gradually reduce to zero due to the progressive interfacial debonding, see Figure 4, right.

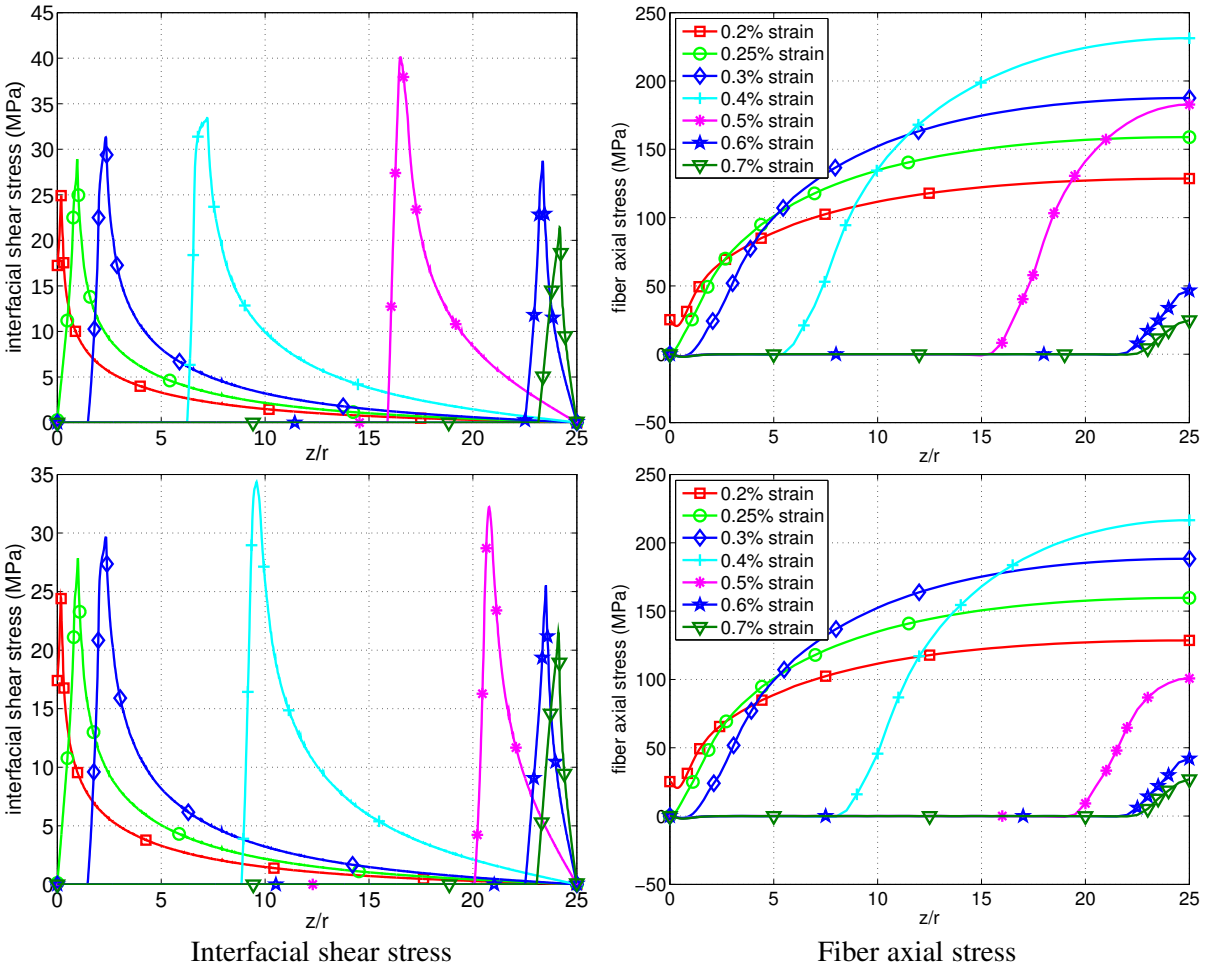


**Figure 4.** Stress profiles of interfacial debonding models with elastic matrix (top) and elastoplastic matrix (bottom). The left two graphs share the legends of the right two.

Moreover, the maximum interfacial shear stress in the model is overestimated (almost twice the IFSS in the elastic model) due to the introduction of viscosity regularization in order to improve convergence [ABAQUS 2008]. The extra shear stress results in overestimation of the fiber axial stress. It is known that the portion of the debonding interface fails to transfer load from the matrix to the fiber. It is expected that the maximum fiber axial stress does not increase once the debonded interface has propagated, if the maximum shear stress does not exceed the interfacial shear strength.

***Comparison of the shear-lag model and the FE model with a perfectly bonded and a debonding interface.*** Stress profiles predicted by the FE model with perfectly bonded and debonded interfaces are compared to that obtained by the shear-lag model [Cox 1952], as shown in Figure 5. The maximum interfacial shear stress from the shear-lag prediction is less than half of the value of the FE results with a perfectly bonded interface. For the debonding model with either an elastic or elastoplastic matrix, the shear stress is zero over the debonded interface region, increases to its maximum value over a small

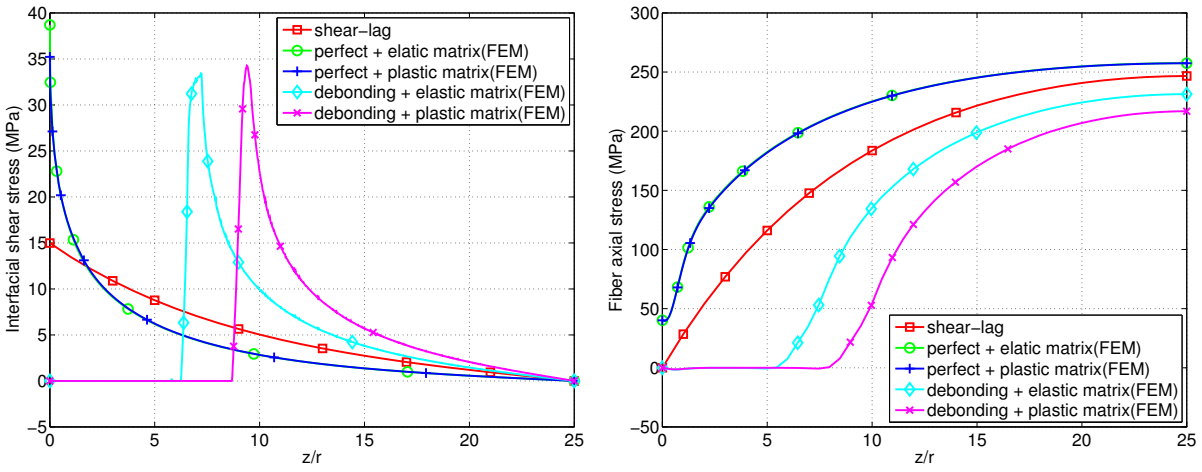


Interfacial shear stress Fiber axial stress

**Figure 5.** Stress profiles of the shear-lag model, the perfectly bonded interface model, and the debonding interface model with elastic and elastoplastic matrices at the same applied strain $\epsilon_m = 0.4\%$.

processing zone, and then decreases exponentially to zero at the fiber midpoint along the fiber length, see Figure 4, left. In contrast, in the perfect interface model with an elastoplastic matrix the shear stress near the fiber-end forms a plateau followed by a bulge containing the maximum shear stress (Figure 3, bottom left). In the perfect interface model with an elastic matrix the shear stress at the fiber tip increases with increasing applied strain level (Figure 3, top left). The fiber axial stress approximates zero over the debonded interface. The maximum axial stress of the fiber predicted by the shear-lag model is less than that of the perfectly bonded interface model, but exceeds that of the debonding interface model (Figure 5, right).

***Effect of matrix plasticity.*** The effect of matrix plasticity on the interfacial shear stress along the fiber interface in the debonding interface model is illustrated in Figure 4, left, for the models with a linear elastic matrix and with a elastoplastic matrix, respectively. The IFSS of $S_2 = 20\,\text{MPa}$ and the toughness of $G_{\text{IIC}} = 100\,\text{J/m}^2$ are kept constant in both cases.

At small applied strain levels, the corresponding stress profiles of both models almost coincide at the same applied strain level (see the curves with the square, circle, and diamond marks in Figure 4, left. As the applied strain level increases and the interfacial debonding propagates, separation of the two corresponding profiles (the curves marked with plus sign and asterisk symbols) implies that the debonding length is different at the same applied strain level for the two models. The debonding length of the elastic model increases slower than that of the plastic model at lower applied strain levels. However, this trend reverses at higher applied strain levels. The total debonding lengths are plotted against different applied strain levels in Figure 6. It is illustrated that the debonding length growth rate (that is, the slope) increases at lower applied strain levels and it decreases at higher applied strain levels for both models. Experimental data of E-glass/epoxy SFC in [Kim and Nairn 2002] show a similar trend of debonding length growth with increasing applied strain. In their work, an applied strain increase from 1.8% (fragmentation) to

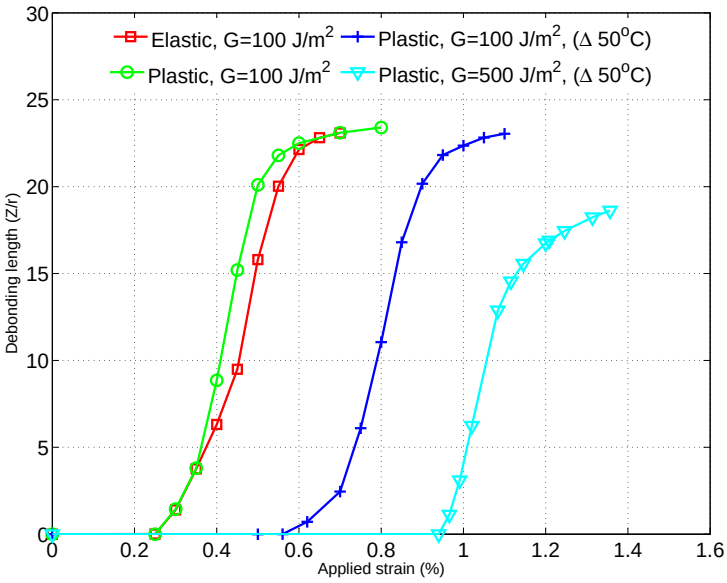


**Figure 6.** Comparison of debonding length at different levels of applied strain of models with an elastic matrix and an elastoplastic matrix and the effect of RTS.

3.3% (a net applied strain increase of 1.5%) caused an increase of $26r$ in the debonding length. In our modeling, an increase of the applied strain from 0.23% to 0.7% (a net applied strain increase of 0.47%) causes an increase of $22r$ in the debonding length. The average debonding growth in our model is faster than that presented in Kim and Narin's results. The discrepancy may be attributed to the low fracture toughness in our model, the absence of frictional force on the interface in our model, and the negligence of the initial RTS effect that will be accounted for in the next section. The frictional force counteracts the interfacial shear stress that drives the interface to damage and failure.

***Effect of the interfacial strength on the debonding process.*** The effect of IFSS within the practical range, $S_2 \in (10, 100)$ MPa, on the debonding process of both the elastic and elastoplastic matrix models is studied, where the toughness of $G_{\mathrm{IIC}} = 100\,\mathrm{J/m^2}$ is kept constant in each case. The parameters and results are tabulated in Table 1. It is shown that the stronger the interfacial strength, the higher the applied strain that is needed to initiate the damage.

It is concluded that the applied strain to initiate the damage of the interface is linearly proportional to the interfacial strength. The increments of applied strain needed to fully damage the first cohesive element along the interface from the fiber end in the elastic model (after the damage is initiated) are 0.22%, 0.17%, and 0.17%, respectively. For the case of $S_2 = 80\,\mathrm{MPa}$, it is 0.16%. Similar results are found in the elastoplastic model. These incremental applied strains are roughly identical (except the first one) since the fracture toughness is kept constant.

***Effect of the interfacial fracture toughness on the debonding process and the stress profiles.*** To study the effect of the interfacial fracture toughness on the debonding process and the stress profiles, three cases are studied. The interfacial shear strengths ($S_2$) of these cases are kept constant (20 MPa), while

| **Effect of IFSS** | | | | |
|---|---|---|---|---|
| ($G_{IIC} = 100\,J/m^2$) | Applied strain to initiate damage | | Applied strain to initiate crack | |
| $\tau_0$ (MPa) | Elastic matrix | Elastoplastic matrix | Elastic matrix | Elastoplastic matrix |
| 10 | 0.04% | 0.04% | 0.26% | 0.25% |
| 20 | 0.07% | 0.07% | 0.24% | 0.24% |
| 30 | — | 0.10% | — | 0.26% |
| 40 | 0.14% | 0.14% | 0.31% | 0.30% |
| 80 | 0.27% | — | 0.43% | — |
| **Effect of fracture toughness** | | | | |
| ($\tau_0 = 20\,MPa$) | Applied strain to initiate damage | | Applied strain to initiate crack | |
| $G_{IIC}$ ($J/m^2$) | Elastic matrix | Elastoplastic matrix | Elastic matrix | Elastoplastic matrix |
| 20 | 0.07% | 0.07% | 0.16% | 0.16% |
| 100 | 0.07% | 0.07% | 0.24% | 0.24% |
| 500 | 0.07% | 0.07% | 0.56% | 0.56% |

**Table 1.** Effect of IFSS and fracture toughness on the debonding process.

the fracture toughnesses ($G_{IIC}$) are set to $20\,J/m^2$, $100\,J/m^2$, and $500\,J/m^2$, respectively. The applied strains to initiate the element damage are all 0.07% while the applied strains to initiate the crack are 0.16%, 0.24%, and 0.56%, respectively. Since the IFSS is below the yield stress of the elastoplastic matrix, the same applied strains are needed to initiate the damage. With increase of the interfacial fracture toughness, a higher applied strain is needed to propagate the crack. The influence of the fracture toughness on the debonding process is also recorded in Table 1.

The interfacial shear stress profiles for these three cases for both models are illustrated in Figure 7. It is observed that the length of the processing zone (where the elements are partially damaged) increases with the interfacial fracture toughness. At the same crack length, the maximum interfacial shear stress of the elastic model is slightly higher than that of the elastoplastic model.

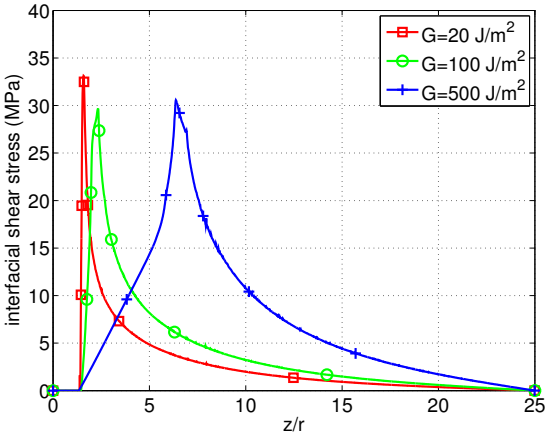


**Figure 7.** Fracture toughness effect on the interfacial shear stress profiles.

## 4. Effect of residual thermal stress

For a piece of material, a change in temperature will result in a contraction or expansion of the material due to its thermal properties. It is commonly seen that RTSs developed in a fiber reinforced composite that has undergone a thermal curing process are due to the mismatch of the CTEs of the fiber and matrix and the constraint of the bonded interface. The generic CTEs for the E-glass fiber and the epoxy matrix are $5 \times 10^{-6}$ /°C and $81 \times 10^{-6}$ /°C, respectively. A temperature drop from an elevated temperature to room temperature during the cooling process is considered in this study. For the model with an elastoplastic matrix and a perfect bonded interface, the RTSs induced by a temperature drop of 50 °C are −20.5 MPa and 33.2 MPa, for the normal stress (compressive) and the shear stress along the interface, respectively. Larger temperature changes will result in higher RTSs. This is a general model used to demonstrate the effect of RTS on the interfacial debonding. The creep effect, which depends on the thermal and mechanical behavior of the matrix and may mitigate the RTS field, however, is not accounted for during the cooling process in this model. The residual thermal shear stress along the perfect interface is shown in Figure 8 (the solid curve without markers).

The residual thermal shear stress developed during the curing process may cause the damage to the interface [Rodriguez 1989]. In the case where the interfacial shear strength equals 20 MPa, the residual thermal shear stress exceeds the IFSS and it causes the damage initiation. As shown in Figure 8 (the dashed curve), the RTS induces damage initiation along the interface with a damage initiation length of $1.8\,r$, for an IFSS of 20 MPa. Moreover, the residual thermal shear stress on the interface is pointing from the fiber tip toward the center of the fiber at the matrix side. Once a tensile strain is applied to the SFC, the RTS needs to be counteracted and then reverse shear stress will develop as the applied strain increases. This results in a higher applied strain level to debond the interface than that in the model without the RTS effect as shown in Figure 8. The combined effect of the RTS and the interfacial fracture toughness is also shown in Figure 6. It needs an even higher applied strain level to debond a tougher

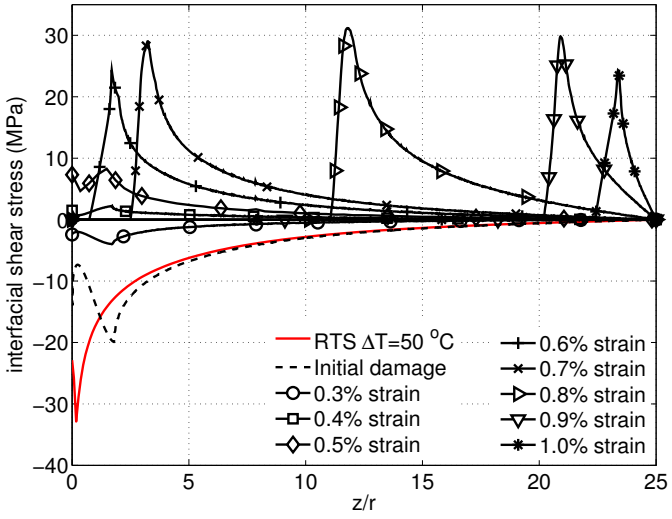


**Figure 8.** Interfacial shear stress with effect residual thermal stress for a debonding interface model.

interface. It is noted that the local (around the debonding tip) elastoplastic matrix becomes softened when the applied strain level reaches about 1.2% in the case where $G_{\mathrm{IIC}}$ equals 500 J/m$^2$ and the RTS effect is considered (the curve marked with $\nabla$s in Figure 6). Instability issues caused by material softening are analyzed using the Riks method implemented in [ABAQUS 2008]. Also to be noted is that when the applied strain increases the crack tip propagates and the matrix on the wake of the crack tip is subjected to unloading. This process enables the propagation of the debonding tip instead of further yielding of the matrix. However, the propagation rate of the crack tip decreases as more external work is consumed in the form of plastic dissipation by the matrix and less external work is used to debond the interface.

Once the RTS effect is considered, an increase of applied strain from 0.56% to 1.1% (a net applied strain increase of 0.54%) causes an increase of $23r$ in the debonding length for $G_{\mathrm{IIC}} = 100$ J/m$^2$. If the RTS and a higher fracture toughness value ($G_{\mathrm{IIC}} = 500$ J/m$^2$) are considered, an increase of applied strain from 0.94% to 1.36% (a net applied strain increase of 0.42%) causes an increase in the debonding length of $18.6r$.

## 5. Conclusions

Finite element results of composite materials consisting of a single short glass fiber (modeled as an isotropic, linear elastic material) with elastic and elastoplastic matrices (characterized by an incremental isotropic hardening model) are presented. Two types of interfaces, perfectly bonded and debonded, are studied. Comparison of the simulation results with published experimental results concludes the following:

- The stress profiles of the debonding interface model differ significantly from those of the perfectly bonded interface model. The interfacial shear stress reduces to zero on the debonded interface. It increases to its maximum value over a small processing zone and decreases exponentially to zero at the fiber midpoint.
- The maximum interfacial shear stress of the elastoplastic matrix model is smaller than that of the elastic matrix model at the same applied strain level.
- For both models, the growth of the debonding length (the slope of the debonding length versus the applied strain curve) increases at lower applied strain levels and decreases at higher applied strain levels.
- The growth of the debonding length in the plastic model is larger than that in the elastic model at small applied strain levels. The trend reverses as the applied strain level increases.
- The applied strain level to initiate the damage of the cohesive element is approximately linearly proportional to the interfacial shear strength.
- When the specimen is subjected to tensile loading, the effect of the residual thermal stress offsets the applied strain level required to initiate damage to the interface, since the residual thermal shear stress needs to be first counteracted so that damage at the interface may occur.

## Acknowledgements

The authors gratefully acknowledge Dr. Carlos G. Dávila of the Langley Research Center for his advice on the cohesive element for the debonding model, and Dr. Ken Chong of the National Science Foundation for his genuine support. This research has been funded by the National Science Foundation, CMMI division.

## References

[ABAQUS 2008] *Abaqus User's Manual*, Version 6.8, Dassault Systèmes/SIMULIA, Providence, RI, 2008.

[Camanho and Dávila 2002] P. P. Camanho and C. G. Dávila, "Mixed-mode decohesion finite elements for the simulation of delamination in composite materials", technical report TM-2002-211737, NASA, 2002, Available at http://paginas.fe.up.pt/demegi/Avaliacao/Pp_Camanho_Davila.pdf.

[Camanho et al. 2003] P. P. Camanho, C. G. Dávila, and M. F. D. Moura, "Numerical simulation of mixed-mode progressive delamination in composite materials", *J. Compos. Mater.* **37**:16 (2003), 1415–1438.

[Carrara and McGarry 1968] A. S. Carrara and F. J. McGarry, "Matrix and interface stresses in a disconinuous fiber composite model", *J. Compos. Mater.* **2**:2 (1968), 222–243.

[Cheng et al. 1993] T.-H. Cheng, F. R. Jones, and D. Wang, "Effect of fiber conditioning on the interfacial shear strength of glass-fibre composites", *Compos. Sci. and Technology* **48** (1993), 89–96.

[Cox 1952] H. L. Cox, "The elasicity and strength of paper and other fiberous materials", *British J. Appl. Phys.* **3** (1952), 72–79.

[Daoust et al. 1993] J. Daoust, T. Vu-Khanh, C. Ahlstrom, and J. F. Gerard, "A finite element model of the fragmentation test for the case of a coated fiber", *Compos. Sci. and Technology* **48** (1993), 143–149.

[Dávila et al. 2008] C. G. Dávila, P. P. Camanho, and A. Turon, "Effective simulation of delamination in aeronautical structures using shells and cohesive elements", *J. Aircraft* **45**:2 (2008), 663–672.

[Galiotis 1993] C. Galiotis, "A study of mechanisms of stress transfer in continuous- and discontinuous-fibre model composites by laser Raman Spectroscopy", *Compos. Sci. and Technology* **48** (1993), 15–28.

[Kim and Nairn 2002] B. W. Kim and J. A. Nairn, "Observations of fiber fracture and interfacial debonding phenomena using the fragmentation test in single fiber composites", *J. Compos. Mater.* **36**:15 (2002), 1825–1858.

[Mandell et al. 1982] J. F. Mandell, D. D. Huang, and F. J. . McGarry, "Crack propagation modes in injection molded fiber reinforced thermoplastics", in *Short fiber reinforced composite materials* (STP 772), edited by B. A. Sanders, ASTM, Philadelphia, 1982.

[Norman and Robertson 2003] D. A. Norman and R. E. Robertson, "The effect of fiber orientation on the toughening of short fiber-reinforced polymers", *J. Appl. Polymer Sci.* **90** (2003), 2740–2751.

[Rodriguez 1989] E. L. Rodriguez, "Microdelamination due to resin shrinkage in filament-wound fibreglass composites", *J. Mater. Sci. Lett.* **8** (1989), 116–118.

[Termonia 1987] Y. Termonia, "Theoretical study of the stress transfer in single fibre composites", *J. Mater. Sci.* **22** (1987), 504–508.

[Tripathi et al. 1996] D. Tripathi, F. Chen, and F. R. Jones, "The effect of matrix plasticity on the stress fields in a single filament composite and the value of interfacial shear strength obtained from the fragmentation test", *Proc. Royal Soc. A* **452**:1946 (1996), 621–653.

[Turon et al. 2005] A. Turon, C. G. Dávila, P. P. Camanho, and J. Costa, "An engineering solution for using coarse meshes in the simulation of delamination with cohesive zone models", technical report TM-2005-213547, NASA, 2005.

[Turon et al. 2007] A. Turon, C. G. Dávila, P. P. Camanho, and J. Costa, "An engineering solution for mesh size effects in the simulation of delamination using cohesive zone models", *Engin. Fracture Mech.* **74** (2007), 1665–1682.

[Yallee and Young 1998] R. B. Yallee and R. J. Young, "Evaluation of interface fracture energy for single-fibre composites", *Compos. Sci. and Technology* **58** (1998), 1907–1916.

Received 14 Apr 2009. Revised 16 Sep 2009. Accepted 21 Sep 2009.

YI PAN: yipan@eden.rutgers.edu
*Department of Mechanical and Aerospace Engineering, Rutgers University, 98 Brett Road, Piscataway, NJ 08854-8058, United States*

ASSIMINA A. PELEGRI: pelegri@jove.rutgers.edu
*Department of Mechanical and Aerospace Engineering, Rutgers University, 98 Brett Road, Piscataway, NJ 08854-8058, United States*
http://cronos.rutgers.edu/∼pelegri/